

Check for updates

Development of 3D Reversible Smart Energy-Saving Devices for Adaptive Energy Management

Ho Jun Jin, Junyong Seo, Ha Uk Chung, Minkyu Jung, Simon Kim, Su Eon Lee, Jun Hyun Park, Jun Seok Choe, Sun-Kyung Kim,* Bong Jae Lee,* Jin-Tae Kim,* and Bong Hoon Kim*

Conventional 2D thin-film-based energy-saving devices face limitations in controlling phase transition temperatures and in material selectivity. In contrast, 3D devices offer better temperature tunability and broader material options for surface coatings. However, existing designs still face challenges like limited deformation and asymmetric structures, hindering adaptation to varying sunlight incidence and azimuth angles. This study proposes symmetric 3D devices incorporating a shape memory alloy actuator, black paint for solar absorption, and a polydimethylsiloxane (PDMS)/Al₂O₂ composite as an RC film, exhibiting the following characteristics: i) reversible, continuously tunable 3D mechanical deformation between solar heating (SH) and radiative cooling (RC) modes via a temperature-responsive actuator; ii) autonomous operation without external power or manual intervention, ensuring energy-saving functionality; and iii) effective operation across diverse climates with durable, flexible, and adaptable design and adjustable transition temperatures for enhanced thermal responsiveness. Theoretical simulations confirm maximum cooling power reduction of 6.8% in summer and heating power reduction of 5.6% in winter. Performance evaluations under varying tilt angles and solar incidence, along with climate simulations across 15 global zones, validate the effectiveness and adaptability of the device for real-world applications. These findings highlight its potential as a scalable, sustainable, energy-efficient solution for future architectural and environmental uses.

1. Introduction

The continuous increase in global energy consumption has created an urgent need for innovative energy-saving technologies, including carbon-neutralization strategies and initiatives such as 100% Renewable Energy (RE100).[1,2] Buildings account for 30-45% of global energy consumption, contributing significantly to critical environmental challenges such as global warming and air pollution.[3-7] In this context, the energy consumption of heating, ventilation, and air conditioning (HVAC) systems varies widely, ranging from 18% to 73% of a building's total energy use, making it a key focus for improving energy efficiency.[7-9] Among the various technologies aimed at reducing energy consumption in buildings, solar thermal harvesting.[10,11] radiative cooling (RC),[12] and other radiation-based heat transfer methods^[13] have emerged as promising solutions due to their efficiency and sustainability. In particular, for RC technology, recent research has focused on the development of innovative

H. J. Jin, S. Kim, S. E. Lee, J. H. Park, J. S. Choe, B. H. Kim Department of Robotics and Mechatronics Engineering DGIST

Daegu 42988, Republic of Korea E-mail: bonghoonkim@dgist.ac.kr

J. Sec

Department of Mechanical and Automotive Engineering Kongju National University Cheonan 3 1080, Republic of Korea



The ORCID identification number(s) for the author(s) of this article can be found under https://doi.org/10.1002/adma.202507682

© 2025 The Author(s). Advanced Materials published by Wiley-VCH GmbH. This is an open access article under the terms of the Creative Commons Attribution-NonCommercial License, which permits use, distribution and reproduction in any medium, provided the original work is properly cited and is not used for commercial purposes.

DOI: 10.1002/adma.202507682

H. U. Chung School of Biomedical Engineering Korea University Seoul 02841, Republic of Korea

M. Jung Technological Collaboration Team 1 HYUNDAI NGV Seoul 08826, Republic of Korea

Seoul 08826, Republic of Korea
S.-K. Kim
Department of Applied Physics
Kyung Hee University
Yongin 17104, Republic of Korea

Yongin 17104, Republic of Ko E-mail: sunkim@khu.ac.kr

B. J. Lee

Department of Mechanical Engineering

Daejeon 34141, Republic of Korea E-mail: bongjae.lee@kaist.ac.kr



materials, such as metasurfaces^[14,15] and organic/inorganic composites,^[16,17] to effectively dissipate excess heat from buildings to outer space through atmospheric transparent windows. These studies have achieved notable success in reducing cooling energy consumption by utilizing materials characterized by low solar absorption and high thermal emissivity. However, most RC devices operate exclusively as cooling systems, which can unintentionally increase heating energy demand when surface temperatures drop below comfort levels, such as during nighttime or winter. To address these limitations, dual-mode smart energy-saving technologies capable of switching between RC and solar heating (SH) have gained notable attention.^[18,19]

Recent advances in 2D thin-film-based smart devices have introduced innovative strategies for dynamic thermal management, including humidity- and temperature-adaptive modulation of refractive indices,[20] voltage-controlled tuning of optical properties, [21] and motor-driven systems. [22] Among these, humidity- and temperature-adaptive methods are particularly appealing because of their simplicity and low energy requirements. Porous materials, such as poly(vinylidene fluorideco-hexafluoropropylene) polymers, [23] cellulose acetate porous coated textile, [24] and porous polytetrafluoroethylene, [25] exhibit humidity-dependent changes in porosity, which modulate solar transmittance through humidity-induced variations in light scattering. This enables reversible transitions between RC and SH modes depending on the humidity level, thereby offering efficient and sustainable thermal management solutions. In addition, VO2-based materials doped with elements such as molybdenum, [26-28] tungsten, [29,30] or strontium[31,32] provide dual-mode thermal regulation capabilities. VO2 undergoes a phase transition between dielectric and metallic states depending on temperature and its critical temperature (T_c) , enabling tunable emissivity control.[33] This unique property facilitates the development of self-regulating thermal management systems.

The applications of these 2D thin-film-based smart materials, such as coatings on building exteriors, show promise for adaptively reducing heating and cooling energy demands. [34-41] However, several challenges hinder their practical implementation, including manufacturing difficulties, limited control of regulating performance owing to a mismatch of the target and phase transition environments, and material constraints in achieving high selectivity of the radiative property spectrum. Addressing these limitations is essential for realizing the full capabilities of film-based smart devices for energy-efficient thermal management. To address these challenges, 3D mechanical actuation offers a promising alternative for enabling transitions between RC and SH modes. [42-51] By harnessing thermal expansion differences between materials, these systems can generate dynamic structural responses to temperature changes. For example, the

J.-T. Kim
Department of Mechanical Engineering
POSTECH
Pohang 37673, Republic of Korea
E-mail: jimmy516@postech.ac.kr

I.-T. Kim

Institute for Convergence Research and Education in Advanced Technology Yonsei University Seoul 03722, Republic of Korea combination of hydrophilic oxidized cellulose and hydrophobic ethyl cellulose enables self-folding mechanisms that open at elevated temperatures and close at lower temperatures.^[44] In such a case, a key advantage is the ability to store solar energy during the day and suppress radiative heat loss at night, offering excellent performance from an energy storage perspective. However, a potential limitation is the dependence on ambient temperature and humidity. Furthermore, thermally responsive polymers or phasechange materials that expand or contract at specific temperature thresholds can facilitate structural deformation and activate radiative cooling or heating functions. For example, thermoresponsive polymers, such as poly(N-isopropylacrylamide), can be utilized to enable on/off dual-mode actuation by exploiting their characteristic volume changes, expanding at elevated temperatures and contracting at lower temperatures depending on ambient conditions. [45] This study also offers the advantage of enabling reversible thermal management modes; however, its drawbacks include potential performance degradation due to the humiditysensitive nature of the polymer, as well as the requirement for complex nanopatterning fabrication processes.

Shape memory alloys can undergo temperature-induced phase transitions accompanied by dimensional changes, offering a promising platform for thermally regulated radiative cooling and heating systems while being unaffected by ambient humidity.[46,51,52] Lee et al.[47] also developed macro- and microscale energy devices capable of reversible dual-mode transitions by harnessing the buckling behavior of polymers induced by mechanical forces. Despite their potential, most existing studies on 3D thermal regulation structures have been limited to controlling motion along a single degree of freedom. However, in outdoor environments, the incidence and azimuth angles of sunlight vary continuously throughout the day and across seasons owing to diurnal solar motion. Consequently, the need for symmetrically designed 3D structures with multidirectional actuation capabilities has been increasingly emphasized to ensure effective light modulation under dynamic solar trajectories. For the same reason, when these structures are deployed on inclined building surfaces for architectural integration, only symmetric structures can maintain the desired optical modulation performance, irrespective of changes in illumination angles. Therefore, it is necessary to develop a modern and smart 3D energy device that can overcome the limitations of the reported 2D thin-film structures and 3D devices.

This study introduces a novel 3D energy-saving device that utilizes a self-driven actuator with an adjustable operating range and overcomes material constraints through the versatility of material coatings with the following key features: i) The devices exhibit reversible 3D mechanical deformation between SH and RC modes, enabled by a temperature-responsive actuator. This device enables continuous tuning across high- and lowtemperature ranges, rather than functioning in a simple binary (on/off) manner. ii) Energy-saving functionality is achieved through autonomous operation without the need for external energy sources or manual adjustments. iii) The system is applicable across diverse climates and regions, offering robustness, versatility, and adaptability to varying environmental conditions. Moreover, the ability to adjust the heating and cooling transition temperatures easily makes the system suitable for development as a personalized thermal regulation platform.





www.advmat.de

The device integrates two specialized surfaces: a carbon blackcoated surface for the SH mode, providing a heating effect exceeding 60 °C above ambient temperature in winter.[47] and an Al₂O₂/PDMS surface for the RC mode, achieving cooling effects as low as -9 °C below ambient temperature in summer.^[53] Mode transitions are regulated by temperature-driven variations in the angle and opening of the wings of the device, inspired by traditional architectural practices that optimize eave angles based on latitude. In this study, the dual-mode thermal management performance of this passive 3D device is validated through theoretical analysis and experimental evaluation. Performance tests conducted at angles of 0° (ground mounted), 45° (slope mounted), and 90° (wall mounted) demonstrated its effectiveness across various surface orientations. Additionally, simulations were conducted to evaluate seasonal performance across different global climates, quantify monthly energy savings, and highlight its potential as a transformative solution for energy management in buildings.

2. Results and Discussion

2.1. Reversible Motion-Enabled 3D Structures for Passive Energy-Saving Devices

Figure 1a,b illustrate the differences in traditional house eave angles based on latitude, comparing the "Hanok" in Seoul, Korea, and "Tingtai Teahouse" in Shanghai, China. In the Northern Hemisphere, traditional houses with steeply angled eaves facing upward are more commonly observed at lower latitudes. This architectural adaptation effectively addresses the need to maintain comfortable indoor temperatures by obstructing sunlight in summer and permitting solar gain. These design strategies are particularly effective at lower latitudes, where the solar altitude angle is higher during winter.^[54] The principles derived from such traditional architectural practices highlight the adaptability of the proposed reversible 3D structures to environmental factors, such as variation in solar irradiance caused by different solar altitudes. These structures demonstrated an effective reduction in cooling/heating energy consumption compared with that of 2D planar structures (Figure 1c).

The proposed 3D device dynamically adjusts its heat transfer pathway depending on the operating mode. In the RC mode, when the ambient temperature increase, the shape memory alloy (SMA) spring expands, causing the RC-coated wings to fold. This configuration maximizes RC in the mid-infrared (MIR) range (8-13 µm, i.e., the atmospheric transparent window range) and reflects incoming solar heat back to the atmosphere. The wings maintain a cold temperature owing to the RC phenomenon, which subsequently cools the underlying surface through convection and radiative heat exchange. In the SH mode, when the temperature drops, the SMA spring contracts, causing the RC wings to open to a 90° angle. This directly exposes the underlying heat-absorbing, black-painted surface to sunlight, thereby enabling solar thermal heating. In the external environment, the wings of the 3D device adjust dynamically based on ambient temperature. Under colder conditions, the wings open and maximize the solar exposure for heating. Conversely, under warmer conditions, the wings close to block sunlight and reduce heat gain, thereby enhancing cooling efficiency. Experimental results

at the baseline room temperature (25 °C) confirmed these adaptive responses. In cold environments (8 °C), the wings fully open, whereas in hot conditions (32 °C), the wings fully close (Figure 1d).

The adaptive 3D device is composed of five primary components: the roof parts, joint parts, support parts, wing frames, wing panels, and SMA spring (Figure 1e). The roof parts are fabricated using a transparent KS158T 3D printing material to effectively capture sunlight, whereas other structural components are fabricated from acrylonitrile butadiene styrene (ABS) 3D printing material. The wing panels feature a dual-layer design, with an outer layer coated with an RC film and an inner layer painted with carbon black for solar absorption. This design allows the wings to interact with sunlight depending on the mode. The RC film, developed in prior research, [53] achieves RC by scattering the solar radiation through alumina (Al₂O₃) nanoparticles and leveraging PDMS as the base material for strong MIR emission. This film exhibits efficient RC performance, is easy to produce, and is wellsuited for applications in 3D devices. The upper surface of the support part is coated with carbon black paint to effectively absorb solar radiation during the SH mode in cold environments. The SMA, composed of a Ni/Ti alloy (nitinol), uses a tension spring with a diameter of 8 mm and a thickness of 1 mm. These components collectively contribute to the adaptive functionality and energy-saving performance of the device (i.e., reduction in energy consumption).

The heating and cooling temperatures of the common surfaces and the proposed 3D device were computed for various external temperatures and coating conditions (Section S1, Supporting Information) based on conventional and detailed heat transfer analysis. Please note that the measured spectral emissivity of coatings (i.e., black paint, urethane coating, and RC film) (Figure S1, Supporting Information). Simulations revealed that black paint and urethane coatings, due to their strong solar absorption, achieved high heating temperatures, while the RC film achieved sub-ambient cooling temperatures through passive cooling phenomena. For the 3D device's bottom surface, we have considered both radiative and convective heat transfer between the variously tilted wings and the bottom surface (Sections 1-2, Supporting Information). A sharp drop in temperature difference above the ambient temperature was observed within the 30-35 °C range, corresponding to the SMA spring's transition range. In addition, as shown in Figure 1, when the ambient temperature increased, the RC mode was gradually activated, resulting in a smaller temperature difference. This behavior enables dynamic switching between cooling and heating modes, providing passive temperature regulation (Figure 1f). As a result, our 3D smart device performed maximal 51.3 °C of heating temperature and 65.7% (i.e., ratio between incoming solar irradiance and the net solar heating power) of solar thermal conversion efficiency at SH mode (i.e., ambient temperature at 6 °C), and minimal -6.1 °C of cooling temperature and 36.1 W m⁻² (i.e., net radiative cooling power) of cooling power at RC mode (i.e., ambient temperature at 40 °C).

Theoretical energy savings were calculated for a conventional building located in Daejeon, South Korea (36.4°N, 127.4°E) using typical meteorological data (Section S2, Supporting Information). The results indicate that the 3D device reduces summer cooling energy consumption (June to August) by 4.9%–6.8% (Figure 1g) and winter heating energy consumption (December to February)

15214095, 2025, 43, Downloaded from https://advanced

l.onlinelibrary.wiley.com/doi/10.1002/adma.202507682 by Dægu Gyeongbuk Institute Of, Wiley Online Library on [03/12/2025]. See the Terms

of use; OA articles are governed by the applicable Creative Commons

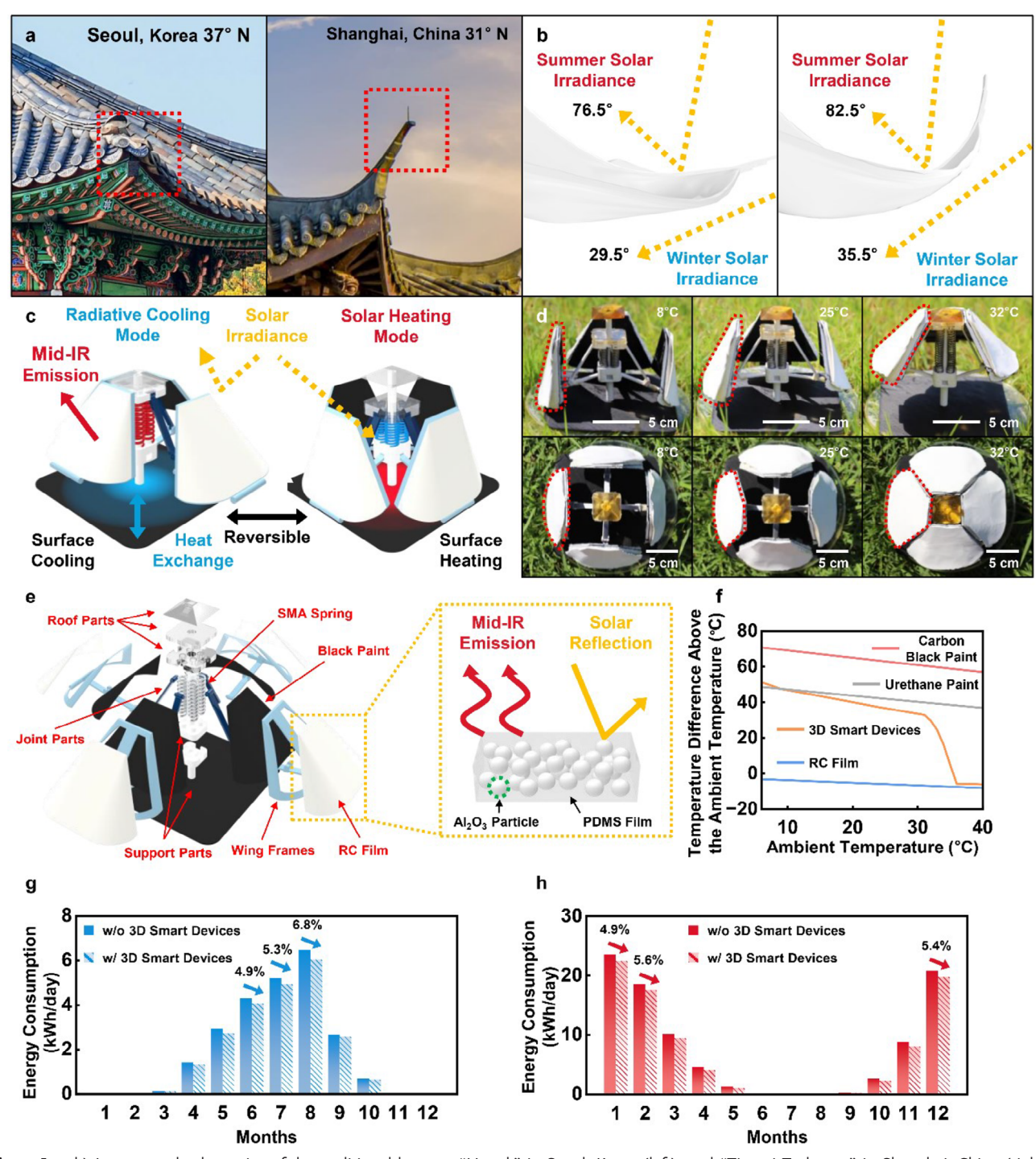


Figure 1. a,b) Images and schematics of the traditional houses: "Hanok" in Seoul, Korea (left), and "Tingtai Teahouse" in Shanghai, China (right). c) Schematic of the 3D smart energy-saving devices. d) Images of the devices in various temperature environments (8, 25, and 32 °C). e) Schematic illustration of the device components. f) Thermal properties of the carbon black paint, urethane paint, radiative cooling film, and 3D smart devices under ambient conditions. Representative performance data with and without the 3D smart energy-saving devices are shown in g) cooling and h) heating modes.





vww.advmat.de

by 4.9–5.6% (Figure 1h). Annual energy savings for other regions were also calculated (Figure S12, Supporting Information). These findings confirm that the proposed 3D device, incorporating an SMA spring, is an effective passive energy-saving solution for cooling and heating applications across various regions, without the need for external power sources.

2.2. Mechanical Characteristics of Passive 3D Energy-Saving Devices

Figure 2a b, provides a schematic of the behavior and operation of the SMA spring in the 3D passive energy-saving device that responds to temperature variations. In a high-temperature environment, the SMA spring elongates, causing the wing frame to rise and the wings to close. In contrast, in a low-temperature environment, the SMA spring contracts, thereby lowering the wing frame and opening the wings. As the SMA length changes with temperature, both the angle between the device's wings and the ground, as well as the opening area, vary accordingly. At \approx 10 °C, the SMA maintains a length of 2.5 cm, whereas at \approx 35 °C, it extends up to 5 cm, demonstrating reversible variability. When the SMA reaches its minimum length, the wing angle increases to a maximum of 90°, with the opening area expanding to 88 cm². Conversely, when the SMA reaches its maximum length, the wing angle decreases to a minimum of 45°, fully closing the opening area and blocking sunlight (Figure 2c).

The forces exerted on the device vary depending on the pushing and pulling forces of the SMA, which change with temperature. As the temperature rises, the SMA expands significantly from ≈30 °C, increasing its pushing force. At 40 °C, the force exerted on the device reaches ≈9.8 N. In contrast, as the temperature decreases, the SMA contracts significantly from \approx 8 °C, generating a pulling force. At 0 °C, the pulling force on the device is \approx 2.5 N. In the force measurement experiment of the SMA, the deviation of the measured data across 10 actuation cycles was less than 0.1 N, confirming that SMA is a mechanically stable material under repeated deformation (Figure 2d,e)[55,56]. The DSC graph reveals the temperature range where the SMA undergoes phase transitions. The shift to the rigid austenite (A) phase begins at \approx 35 °C, correlating with the increasing pushing force shown in Figure 2d. As the temperature decreases, the SMA transitions through the intermediate rhombohedral (R) phase before reaching the softer martensite (M) phase. The transition to the M phase starts at ≈4 °C, aligning with the increasing pulling force shown in Figure 2e (Figure 2f). The SMA exhibited minimal variation in phase transformation temperatures and hysteresis after 10 DSC cycles, demonstrating its superior thermal durability (Figure \$7, Supporting Information)[55,56].

The opening area of the device was estimated based on the temperature of the SMA spring under summer and winter conditions. Assuming that the SMA spring temperature matched the ambient temperature, the relationship between the SMA spring length and temperature (Figure S4, Supporting Information), along with the correlation between the SMA spring length and opening area (Figure 2c), was used to obtain the simulation results. Predicting variations in the opening area under the hottest (i.e., approximately noon on August 7) and coldest (i.e., approximately dawn on January 24) conditions in Daejeon, South Ko-

rea, the analysis confirms significant changes in the opening area when the ambient temperature reaches the SMA transformation temperature range (i.e., 30–36 °C). This suggests that, when applied in an actual environment, the 3D device will dynamically switch between cooling and heating modes (Figure 2g). However, in cold weather, the opening area remains open, keeping the device in heating mode (Figure 2h).

The outdoor temperature and corresponding opening area of the 3D device were measured over 9 days in August 2024 in Daejeon to validate its performance under summer conditions and to investigate other external factors such as solar irradiance and heat conduction to surrounding components. At night, the device remained open, as expected, while during the day, the 3D structure closed earlier than the theoretical value of 36 °C, activating the cooling mode. These results indicate that increased solar irradiance preheats the SMA spring. This characteristic enhances the energy-saving function of the passive 3D device for building heating and cooling, as the activation temperature for cooling mode closely aligns with a building's thermal management target temperature (e.g., ≈20–24 °C). [4,57] The findings highlight the effective energy-saving performance of the device and the importance of external factors such as solar irradiance in optimizing its functionality (Figure 2i).

2.3. Performance Testing of the Device on Surfaces at Various Angles

Figure 3a b, presents a schematic and image of the outdoor experimental setup for the 3D passive device, respectively. The performance comparison under different tilt angles [0° (ground mounted), 45° (slope mounted), and 90° (wall mounted)] and material configurations highlights the versatility of the device and the critical influence of the manufacturing materials. The material combinations include carbon black paint only, RC paint only, urethane paint only, and the reversible 3D device. The theoretically predicted temperature variations for the lower surface of the reversible 3D device under summer and winter conditions, based on the ambient temperature data, are shown in Figure 3c,d, respectively.

Consistent with the previous findings in Figure 2g,h, the ambient temperature during summer fluctuates around the SMA transformation temperature, leading to alternating activation of the cooling and heating modes. As shown in Figure 3d, during winter, the low ambient temperature caused the SMA spring to contract and continuously maintain the heating mode (Figure 3c,d). Temperature measurements across different tilt angles and material configurations further demonstrated the effective temperature regulation properties for broad applications, such as rooftop, slope, and walls (Figure 3e-g).[58] Notably, the temperature of the 3D device (i.e., orange-colored line) was collected by measuring the point beneath the 3D device's bottom surface, and the 3D smart device blades (i.e., purple-colored line) were determined by measuring the surface beneath the wings of the device. Around noon, the SMA spring has not yet been activated, keeping the 3D device in heating mode. This results in a higher surface temperature than that of the RC-coated surface. This observation also implies that the heating mode activation of the 3D smart devices can be expected. However, as the

www.advmat.de

15214095, 2025, 43, Downloaded from https://advanced.onlinelibrary.wikey.com/doi/10.1002/adma.202507682 by Dægu Gyeongbuk Institute Of, Wiley Online Library on [03/12/2025]. See the Terms and Conditions (https://onlinelibrary.com/doi/10.1002/adma.202507682 by Dægu Gyeongbuk Institute Of, Wiley Online Library on [03/12/2025]. See the Terms and Conditions (https://onlinelibrary.com/doi/10.1002/adma.202507682 by Dægu Gyeongbuk Institute Of, Wiley Online Library on [03/12/2025]. See the Terms and Conditions (https://onlinelibrary.com/doi/10.1002/adma.202507682 by Dægu Gyeongbuk Institute Of, Wiley Online Library on [03/12/2025]. See the Terms and Conditions (https://onlinelibrary.com/doi/10.1002/adma.202507682 by Dægu Gyeongbuk Institute Of, Wiley Online Library on [03/12/2025]. See the Terms and Conditions (https://onlinelibrary.com/doi/10.1002/adma.202507682 by Dægu Gyeongbuk Institute Of, Wiley Online Library on [03/12/2025]. See the Terms and Conditions (https://onlinelibrary.com/doi/10.1002/adma.202507682 by Dægu Gyeongbuk Institute Of, Wiley Online Library on [03/12/2025]. See the Terms and Conditions (https://onlinelibrary.com/doi/10.1002/adma.202507682 by Dægu Gyeongbuk Institute Of, Wiley Online Library on [03/12/2025]. See the Terms and Conditions (https://onlinelibrary.com/doi/10.1002/adma.202507682 by Dægu Gyeongbuk Institute Of, Wiley Online Library on [03/12/2025]. See the Terms and Conditions (https://onlinelibrary.com/doi/10.1002/adma.202507682 by Dægu Gyeongbuk Institute Of, Wiley Online Library on [03/12/2025]. See the Terms and Conditions (https://onlinelibrary.com/doi/10.1002/adma.202507682 by Dægu Gyeongbuk Institute Of, Wiley Online Library on [03/12/2025]. See the Terms and Conditions (https://onlinelibrary.com/doi/10.1002/adma.202507682 by Dægu Gyeongbuk Institute Of, Wiley Online Library on [03/12/2025]. See the Terms and Conditions (https://onlinelibrary.com/doi/10.1002/adma.202507682 by Dægu Gyeongbuk Institute Of, Wiley Online Library on [03/12/2025]. See the Terms and Conditions (https:

xonditions) on Wiley Online Library for rules of use; OA articles are governed by the applicable Creative Commons License

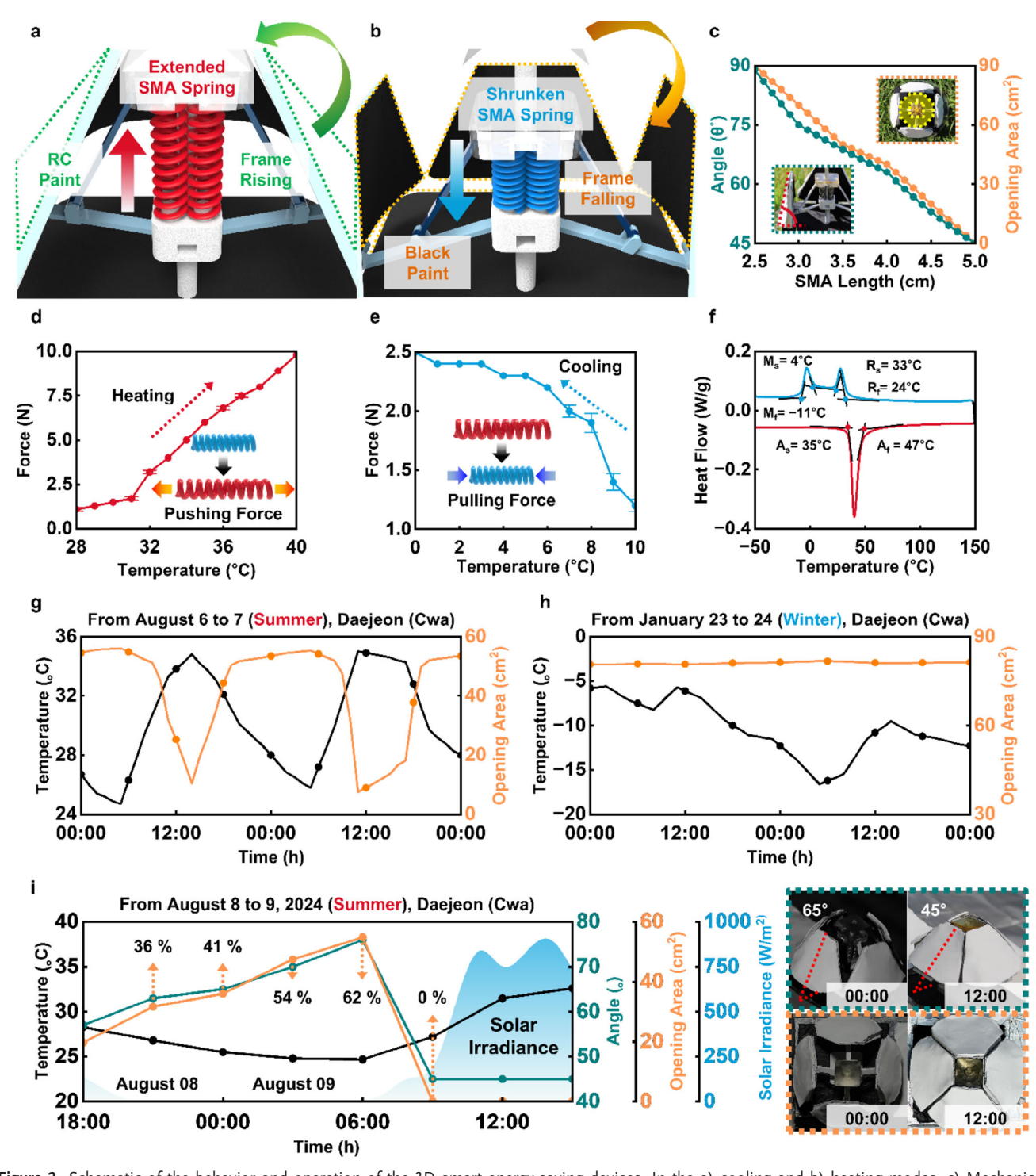


Figure 2. Schematic of the behavior and operation of the 3D smart energy-saving devices. In the a) cooling and b) heating modes. c) Mechanical properties of the 3D smart devices: wing angle and opening area based on the Shape Memory Alloy (SMA) length. Thermal properties of the SMA: d) pushing force under heating conditions, e) pulling force under cooling conditions, and f) DSC data. Mechanical properties of the 3D smart devices: temperature-dependent opening area in g) summer and h) winter. i) Time-resolved mechanical response of the 3D smart devices: wing angle and opening area over 24 h.

www.advmat.de

15214095, 2025, 43, Downloaded from https://advancec

onlinelibrary.wiley.com/doi/10.1002/adma.202507682 by Dægu Gyeongbuk Institute Of, Wiley Online Library on [03/12/2025]. See the Terms

of use; OA articles are governed by the applicable Creat

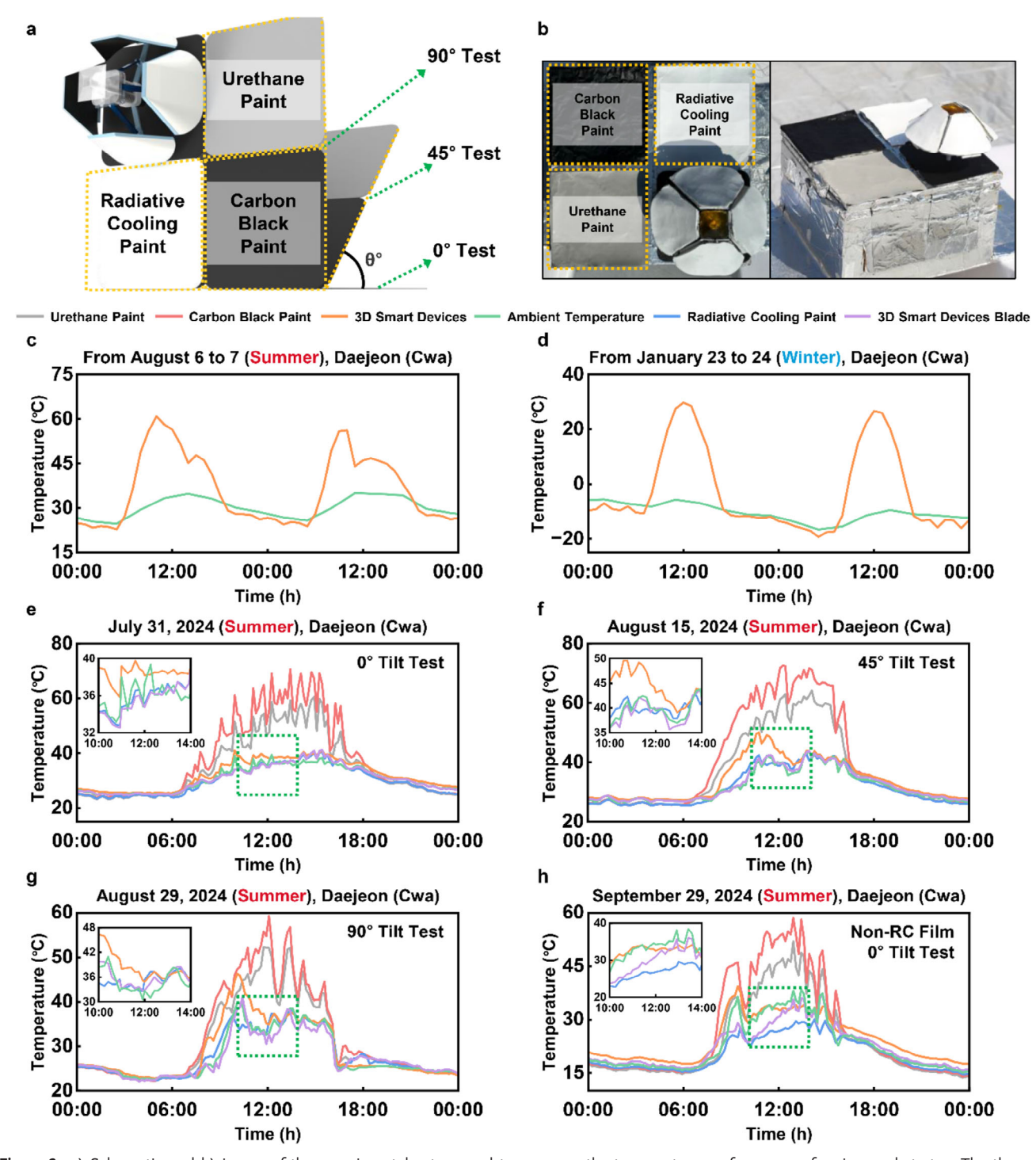


Figure 3. a) Schematic and b) image of the experimental setup used to measure the temperature performance of various substrates. The thermal properties of the 3D smart devices in c) summer and d) winter are shown. The thermal properties of various substrates in e) 0° , f) 45° , g) 90° , and h) 0° are presented without a radiative cooling film. The curves represent urethane paint (black line), carbon black paint (red line), 3D smart devices (orange line), ambient temperature (green line), radiative cooling paint (blue line), and the blade component of the 3D smart devices (purple line).



ADVANCED MATERIALS

www.advmat.de

temperature increases sufficiently, the device transitions to the cooling mode, gradually cooling down until its lower surface temperature aligns with that of the RC-coated surface across all tilt angles.

An identical experiment with a non-RC-coated version of the 3D device further confirmed the crucial role of the RC wings (Figure 3h). Unlike the RC-coated device, the non-RC version did not cool down as effectively, even after the cooling mode was fully activated at around noon. This indicates that the thermal exchange between the cooled RC surface and the lower surface of the device plays a crucial role in its temperature regulation mechanism. Consequently, these findings suggest that a combination of high-cooling and high-heating materials is essential to achieve optimal temperature regulation. This performance test was conducted over multiple days, and the results are provided in Figure S10 (Supporting Information).

2.4. Simulation-Based Estimation of Energy Savings Using the 3D Smart Device Under Various Climate Conditions

Since a massive production of the 3D smart device for experimental validation with it was practically impossible, a theoretical simulation was conducted to evaluate the energy-saving potential of the proposed 3D smart device quantitatively.^[59] The energy consumption was assessed by comparing the HVAC loads of a conventional building with and without the 3D device. Figure 4a illustrates the simulation model for heat exchange in a typical building. Following a simplified 0D numerical model from the previous study,^[59] various heat transfer components were considered, including heat exchange through the walls (q_{walls}) , floors (q_{floors}) , windows $(q_{windows})$, ventilation (q_{vent}) , and rooftop (q_{roof}) . These heat transfer processes occur naturally, leading to indoor temperature fluctuations that require additional thermal management via heat pump (HP) operation (q_{HP}). The energy required to operate the HP is determined by $W_{HP} = q_{HP}/COP$, where W_{HP} represents the electrical power consumed by the HP and COP represents the coefficient of the HP performance (Section S2, Supporting Information).

The application of the 3D smart device to a building's rooftop modulates the roof temperature in response to ambient conditions, altering the q_{roof} and reducing the heat exchange between the roof and indoor space. Consequently, the required heating and cooling energy (q_{HP}) and the corresponding power consumption (W_{HP}) decrease, leading to enhanced energy efficiency. Figure 4b presents a schematic of the 3D device array installed on a rooftop, illustrating the heat transfer mechanisms involved. During the cooling mode (i.e., when the opening area is minimal), net RC occurs on the wing surfaces, thereby reducing their temperatures. Consequently, heat is extracted from the rooftop surface via radiative and convective heat exchange. As the ambient temperature decreases, the device transitions from cooling to heating mode (i.e., the opening area increases), which allows solar radiation to penetrate through the openings and be absorbed by the black-painted surfaces for thermal conversion. This dynamic adjustment enables adaptive rooftop temperature modulation and optimizes energy efficiency without active mechanical intervention (Sections S1, S2, Supporting Information).

Before conducting the building energy consumption simulation, a simple calculation of the climate-dependent activation of the 3D device was performed to guarantee its feasibility. A "mode ratio" was defined as the proportion of time the device operates in each operational mode. The opening area ratios for the cooling, transition, and heating modes were 0-20%, 20-80%, 80-100%, respectively. The mode ratio was calculated using annual ambient temperature data for each city combined with the temperatureopening area relationship established in Figure 2. The mode ratio calculations were performed for 15 representative cities worldwide, selected based on the Köppen-Geiger climate classification (Figure 4e).[60] Please note that the 15 cities were selected to be nearly-uniformly distributed on Earth, since there are similar heating and cooling loads under the same climate classification due to the criteria.^[58] Among the 15 cities, 4 representative climates were selected for comparison: i) Puerto Ayacucho, Venezuela (Am climate: tropical monsoon), ii) Moscow, Russia (Dfb climate: cold and snowy regions), iii) Los Angeles, USA (BSk: cold semi-arid), and iv) Kufra, Libya (BWh: hot desert), as shown in Figure 4c,d,f,g, respectively. As expected, in Am climates, the device remained predominantly in cooling mode (Figure 4c), assisting in offsetting the high cooling demand. In Dfb climates, the heating mode dominated, supporting heat retention (Figure 4d). In the BSk and BWh climates, frequent transitions occur between the heating and cooling modes. Owing to the higher annual temperature fluctuations in BWh climates, both cooling and heating modes were actively engaged, whereas transition modes dominated in BSk climates. These findings suggest that 3D smart devices have the potential for effective thermal regulation across various climatic conditions, enabling daily, monthly, and annual thermal management without external energy input. Figure 4h,i illustrate the annual heating and cooling energy consumption for buildings with and without the 3D device in the four representative cities.

Energy consumption for an additional 11 regions was also calculated (Figure S12, Supporting Information). The results demonstrate that the 3D device effectively reduces energy consumption across all climates. In regions with high cooling demands, cooling energy savings of 9.1% and 17.0% were achieved in the Am and BWh climates, respectively. In colder regions, such as Dfb, the heating energy consumption decreased by 4.6%. The lower heating energy savings compared to cooling savings can be attributed to insufficient solar energy availability in high-latitude regions, where a lower solar altitude limits effective heat absorption. However, in the BSk and BWh climates, where solar energy is more abundant, higher heating energy savings (≈16%) were observed owing to their lower latitudes. Both cooling and heating energy savings for BWh climates exceeded those for BSk climates because of the extreme annual temperature fluctuations in BWh climates. These results further highlight the 3D reversible smart device's ability to adaptively regulate temperature and achieve significant energy savings, regardless of climate, location, and time. Because of its non-motorized, selfregulating thermal management capabilities, this device offers an efficient solution for reducing building energy consumption, making it a promising technology for sustainable construction applications.

www.advmat.de

15214095, 2025, 43, Downloaded from https://advanced.onlinelibrary.wiley.com/doi/10.1002/adma.202507682 by Dægu Gyeongbuk Institute Of, Wiley Online Library on [03/12/2025]. See the Terms

of use; OA articles are governed by the applicable Creative Commons License

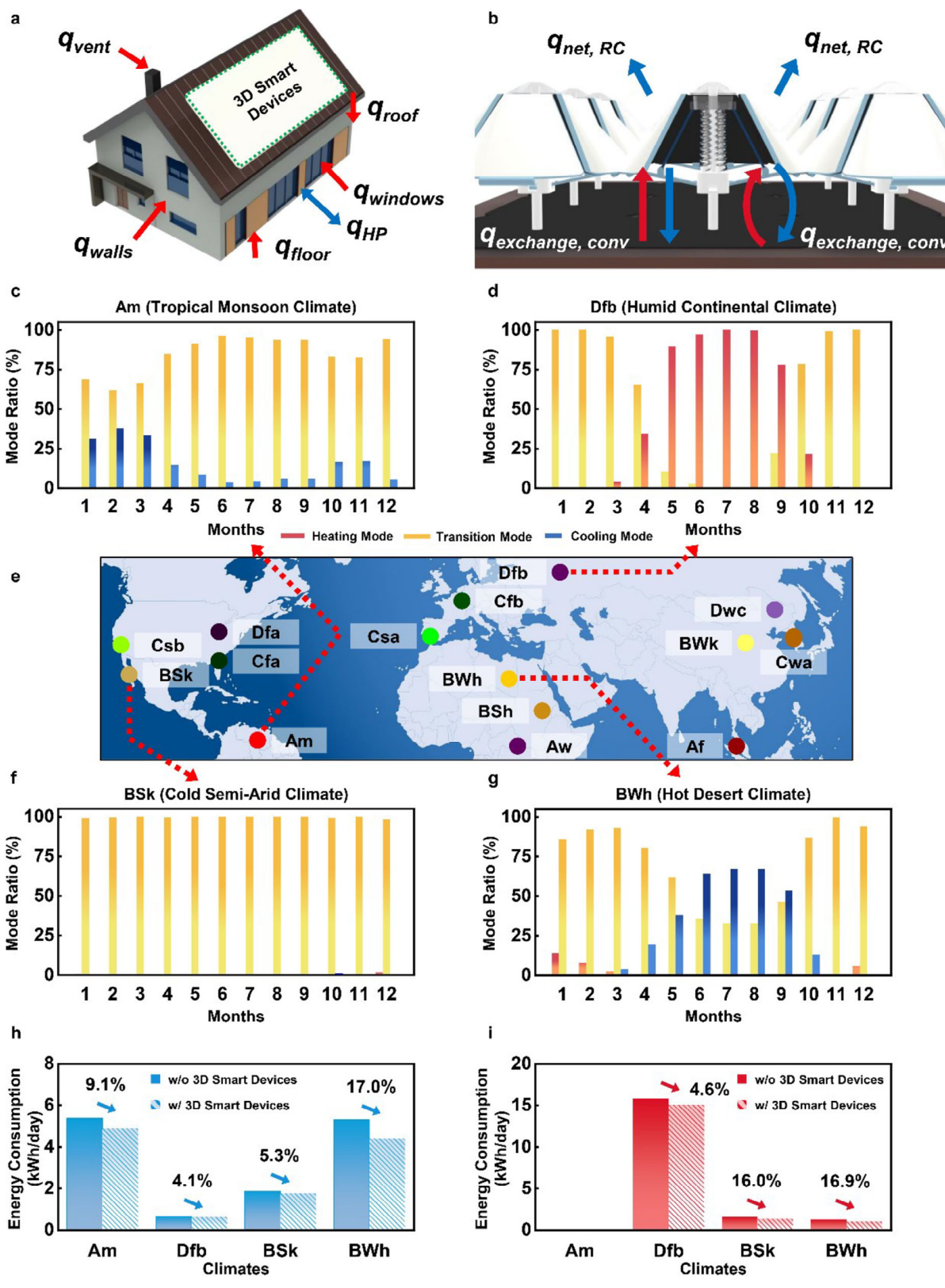


Figure 4. a) Schematic of the simulation model for heat exchange in a typical building. b) Schematic of the 3D device array installed on a rooftop, illustrating the heat transfer mechanisms. The mode ratio of the 3D smart devices in the c) Am climate, d) Dfb climate, f) BSk climate, and g) BWh climate is shown. e) Schematic of the 15 representative cities worldwide, selected based on the Köppen–Geiger Climate Classification. The energy-saving performance data of the 3D smart energy-saving devices in the h) cooling and i) heating modes for four representative regions are shown.

1521495, 2025, 43, Downloaded from https://advanced.on/inelibrary.wiley.com/doi/10.1002/adma.202507682 by Daegu Gyeongbuk Institute Of, Wiley Online Library on [03/12/2025]. See the Terms and Conditions (https://onlinelibrary.wiley.com/terms-and-conditions) on Wiley Online Library or rules of use; OA articles are governed by the applicable Creative Commons License

www.advancedsciencenews.com

ADVANCED MATERIALS

3. Conclusion

In this study, a 3D building energy-saving device utilizing an SMA-based actuator is proposed. This device enables energy reduction in buildings without external power consumption. When combined with conventional building construction strategies, this approach proves applicable across various climates and environmental conditions, both spatially and temporally. The unique 3D structure of the device effectively adapts to variations in solar intensity and incident angles due to latitude, addressing the challenges faced by previous energy-saving devices. The effectiveness and versatility of the 3D smart energy-saving device were validated through real-world temperature measurements and climate simulations across different times of day, seasons, and geographic locations. Additionally, performance tests on surfaces with varying tilt angles and material configurations confirmed the device's capability to enhance energy efficiency across diverse architectural designs. This energy-saving strategy has significant potential for future development, particularly by adjusting the SMA activation temperature to enable customized functionality tailored to user requirements, making it a highly adaptable solution for sustainable building applications.

4. Experimental Section

Fabrication of $Al_2O_3/PDMS$ Radiative Cooling Surface: The $Al_2O_3/PDMS$ mixture for the RC coating was fabricated using the following procedure [53] 1) The PDMS base, curing agent (Sylgard 184 A and B, Dow Corning), and 500 nm Al_2O_3 particles (DT-ALO-S45, Ditto Technology) were mixed in a designated mass ratio (i.e., 1:2:5) for optimal cooling performance [53] and stirred by hand for least 20 min; 2) The mixture was applied to the target surface, such as a, wing surface or Al foil; 3) The applied product was degassed in a low-level vacuum chamber for over 30 min to eliminate air bubbles; 4) The degassed product was thermally cured in a convection oven at 50 °C for more than 15 h. The fabrication process is described in detail in the literature. [53]

Fabrication of 3D Smart Energy-Saving Devices: The framework components of the 3D smart devices were made from ABS materials and fabricated using a Zortrax M300 3D printing system. The roof components of the 3D smart devices were composed of KS158T SLA materials and fabricated using a Kings SLA 600 3D printing system. The SMA springs, used as actuators in the 3D device, were fabricated using materials supplied by SE Corporation. The inner surface of the wing frames was coated with carbon black paint, while the outer surface was covered with an RC film. Subsequently, the frames were integrated with the support components. The roof components and wing frames were assembled using joint elements. Finally, the SMA springs were inserted into the grooves of the support components, thereby completing the assembly of the 3D smart energy-saving devices.

Measurement of Thermal Properties of SMA Springs: The thermal properties were measured using the following commercial instruments: force gauge (AMF-50, Shahe), SEM EDS (GeminiSEM 300, Carl Zeiss), DSC (Discovery DSC, TA Instruments), hermetic pan, and thermogravimetric analysis with an Auto Q500 (TA Instruments).

Measurement of 3D Smart Device's Outdoor Temperature: The temperature of the bottom surface of the 3D smart device was measured using a K-type thermocouple (TC; OMEGA). The tip of the TC was attached below the support of the 3D device (i.e., between the support part and the floor surface). Time-variant temperature signals from the TC were collected using a data logger (GL820, Graphtec) at 1-min intervals. Notably, the temperatures of the surfaces (i.e., the bottom surface of the 3D device and the surfaces with other coatings, such as black paint, urethane paint, and RC coating) were uniformly distributed, as the surfaces were thin and the overall thermal capacitance was negligible.

Measurement of Spectral Emissivity: The emissivity spectra were measured using the following commercial spectrometers and corresponding integrating spheres, depending on the spectral regimes: UV–vis spectrometer (UV-3600i Plus, Shimadzu) with ${\rm BaSO_4}$ integrating sphere (ISR-603, Shimadzu) for 0.3–2.5 μm , and Fourier-transform infrared spectrometer (Nicolet iS50, ThermoFisher) with gold integrating sphere (Mid-IR IntegratIR, PIKE Technologies) for 2.5–15.0 μm .

Supporting Information

Supporting Information is available from the Wiley Online Library or from the author.

Acknowledgements

H.J.J. and J.S. contributed equally to this work. This study was supported by the National Research Foundation of Korea (NRF) grant funded by the Korean Government (MSIT) (No. 2022M3H4A1A02046445, No. RS-2024-00347619, No. RS-2024-00406240, and No. RS-2024-00407155).

Conflict of Interest

The authors declare no conflict of interest.

Data Availability Statement

The data that support the findings of this study are available from the corresponding author upon reasonable request.

Keywords

3D structures, dual-mode thermal management, energy saving, passive operation, radiative cooling

Received: April 23, 2025 Revised: June 15, 2025 Published online: July 7, 2025

- [1] M. Burke, S. M. Hsiang, E. Miguel, Nature 2015, 527, 235.
- [2] A. Q. Al-Shetwi, I. Z. Abidin, K. A. Mahafzah, M. Hannan, J. Clean. Prod. 2024, 478, 143942.
- [3] M. O. Farghali, A. I. Mohamed, I. M. A. Chen, Z. Chen, L. Ihara, I. Yap, P.-S. Rooney, D. W. Rooney, Environ. Chem. Lett. 2023, 21, 2003.
- [4] L. Pérez-Lombard, J. Ortiz, C. P. Pout, Energy Build. 2008, 40, 394.
- [5] K. Parvin, M. Hossain, A. Arsad, P. J. Ker, M. Hannan, J. Build. Eng. 2025, 100, 111795.
- [6] H. Zhang, S. Seal, D. Wu, F. Bouffard, B. Boulet, IEEE Access 2022, 10, 27853.
- [7] X. Cao, X. Dai, J. Liu, Energy Build. 2016, 128, 198.
- [8] M. Balbis-Morejon, J. J. Cabello-Eras, J. M. Rey-Hernandez, C. Isaza-Roldan, F. J. Rey-Martínez, Alexandria Eng. J. 2023, 69, 469.
- [9] M. González-Torres, L. Pérez-Lombard, J. F. Coronel, I. R. Maestre, D. Yan, Energy Rep 2022, 8, 626.
- [10] L. A. Omeiza, M. Abid, A. Dhanasekaran, Y. Subramanian, V. Raj, K. Kozak, U. Mamudu, A. K. Azad, J. Eng. Res. 2023, 12, 994.
- [11] M. S. Buker, S. B. Riffat, Renew. Sustain. Energy Rev. 2015, 51, 327.
- [12] K. Huang, Z. Huang, Y. Du, Y. Liang, J. Liu, J. Yan, J. Mater. Chem. A 2024, 12, 28682.



www.advmat.de

- [13] Y. H. Chan, Y. Zhang, T. Tennakoon, S. C. Fu, K. C. Chan, C. Y. Tso, K. M. Yu, M. P. Wan, B. L. Huang, S. Yao, *Energy Convers. Manag.* 2022, 272, 116342.
- [14] Y. Zhai, Y. Ma, S. N. David, D. Zhao, R. Lou, G. Tan, R. Yang, X. Yin, Science 2017, 355, 1062.
- [15] R. Ali, W. Su, M. Ali, A. Akhtar, M. Usman, Z. U. Khan, Sol. Energy Mater. Sol. Cells 2025, 286, 113591.
- [16] Y. Du, W. Wang, J. Mei, L. Zhang, Chem. Eng. J. 2024, 485, 149976.
- [17] G. Perrakis, A. C. Tasolamprou, G. Kenanakis, E. N. Economou, S. Tzortzakis, M. Kafesaki, ACS Photonics 2022, 9, 1327.
- [18] S. Zhou, P. Chen, C. Xiao, Y. Ge, H. Gao, RSC Adv. 2023, 13, 31738.
- [19] X. Yang, Y. Yang, L. Chen, L. Zhu, W. Yu, Z. Zeng, Chem. Eng. J. 2024, 494, 152920.
- [20] M. Ono, K. Chen, W. Li, S. Fan, Opt. Express 2018, 26, A777.
- [21] Z. Zhang, X. He, M. Yu, L. Zhang, X. Xiao, C. Zou, Y. Gao, Q. Wang, H. Yang, J. Mater. Chem. A 2024, 12, 25773.
- [22] X. Li, B. Sun, C. Sui, A. Nandi, H. Fang, Y. Peng, G. Tan, P.-C. Hsu, Nat. Commun. 2020, 11, 6101.
- [23] H. Ju, S. Lei, F. Wang, D. Yang, J. Ou, A. Amirfazli, Energy Build. 2023, 292, 113184.
- [24] S. Zhang, F. Zhang, J. Su, J. Han, Prog. Org. Coat. 2024, 197, 108772.
- [25] Z. Luo, B.-X. Li, H. Sun, J. Liu, H.-Y. Zhao, Z.-Z. Yu, D. Yang, J. Mater. Chem. A 2023, 11, 16595.
- [26] G. Khan, K. Asokan, B. Ahmad, Thin Solid Films 2017, 625, 155.
- [27] F. Chen, L. Yuan, X. Wu, Y. Huang, Y. Wang, X. Weng, Ceram. Int. 2023, 49, 25585.
- [28] J. H. Park, J. H. Kim, S. E. Lee, H. Kim, H. Y. Lim, J. S. Park, T. Yun, J. Lee, S. Kim, H. J. Jin, Adv. Fiber Mater. 2024, 6, 1813.
- [29] G. Hunt, J. Miragliotta, L. Oh, J. Ginn, A. Warren, D. Shrekenhamer, Proc. SPIE 2022, 12195, 121380J.
- [30] C. Kim, S. Lee, J. Hwang, J. Yoon, J. Sens. Sci. Technol. 2025, 34, 138.
- [31] Y. Liu, Y. Tian, X. Liu, F. Chen, A. Caratenuto, Y. Zheng, Appl. Phys. Lett. 2022, 120.
- [32] D.-g. Lee, S.-b. Kim, Y. Yan, S. Hur, H.-c. Song, J. Sens. Sci. Technol. 2025. 34, 116.
- [33] A. V. Ilinskiy, R. Kastro, M. Pashkevich, E. Shadrin, Semiconductors 2020, 54, 403.
- [34] Y. Rao, J. Dai, C. Sui, Y.-T. Lai, Z. Li, H. Fang, X. Li, W. Li, P.-C. Hsu, ACS Energy Lett. 2021, 6, 3906.
- [35] S. Seo, M. Min, S. M. Lee, H. Lee, Nat. Commun. 2013, 4, 1920.
- [36] K. R. Pyun, S. Jeong, M. J. Yoo, S. H. Choi, G. Baik, M. Lee, J. Song, S. H. Ko, Small 2024, 20, 2308572.

- [37] J. Fei, D. Han, J. Ge, X. Wang, S. W. Koh, S. Gao, Z. Sun, M. P. Wan, B. F. Ng, L. Cai, Adv. Funct. Mater. 2022, 32, 2203582.
- [38] M. Shi, Z. Song, J. Ni, X. Du, Y. Cao, Y. Yang, W. Wang, J. Wang, ACS Nano 2023, 17, 2029.
- [39] M. Liu, X. Li, L. Li, L. Zhao, S. Lu, K. Chen, K. Zhu, J. Zhou, T. Hu, C. Changlong, ACS Nano 2023, 17, 9501.
- [40] K. Sun, W. Xiao, C. Wheeler, M. Simeoni, A. Urbani, M. Gaspari, S. Mengali, C. H. De Groot, O. L. Muskens, *Nanophotonics* 2022, 11, 4101
- [41] J. Huang, X.-k. Zhang, X. Yu, X. Tang, G. H. Wang, X. Du, M. Mu, Renew. Energy 2024, 224, 120208.
- [42] Q. Zhang, Y. Lv, Y. Wang, S. Yu, C. Li, R. Ma, Y. Chen, *Nat. Commun.* 2022, 13, 4874.
- [43] Y. Liu, R. Liu, J. Qiu, S. Wang, J. Adv. Manuf. Process. 2022, 4, 10107.
- [44] R. Liu, J. Li, J. Duan, B. Yu, W. Xie, B. Qi, H. Wang, X. Zhuang, S. Liu, P. Liu, Cell Rep. Phys. Sci. 2021, 2, 100533.
- [45] W. Wang, Z. Zhao, Q. Zou, B. Hong, W. Zhang, G. P. Wang, J. Mater. Chem. C 2020, 8, 3192.
- [46] Z. Xia, Z. Fang, Z. Zhang, K. Shi, Z. Meng, ACS Appl. Mater. Interfaces 2020, 12, 27241.
- [47] S. E. Lee, J. Seo, S. Kim, J. H. Park, H. J. Jin, J. Ko, J. H. Kim, H. Kang, J. T. Kim, H. Lee, Adv. Mater. 2024, 36, 2400930.
- [48] Y. An, Y. Fu, J.-G. Dai, X. Yin, D. Lei, Cell Rep. Phys. Sci. 2022, 3, 101098.
- [49] J. H. Lee, S. K. Jeon, J. Sens. Sci. Technol. 2025, 34, 76.
- [50] S. E. Lee, H. Lee, J. H. Kim, J. C. Park, S. Kyung, H. Choi, S. H. Baek, J. H. Park, S. Park, J.-M. Kim, npj Flex. Electron. 2024, 8, 65.
 - [51] Q. Ye, N. Guo, M. Chen, Appl. Phys. Lett. 2025, 126.
 - [52] N. Guo, C. Shi, N. Warren, E. A. Sprague-Klein, B. W. Sheldon, H. Yan, M. Chen, Adv. Energy Mater. 2024, 14, 2401776.
- [53] S. Yoon, J. Seo, J. Jung, M. Choi, B. J. Lee, J. B. Kim, Int. J. Heat Mass Transf. 2024, 227, 125574.
- [54] D.-K. Kim, Build. Environ. 2006, 41, 1905.
- [55] S.-K. Wu, Y.-C. Chang, Mater. 2019, 12, 2512.
- [56] K. Senthilnathan, A. Shamimi, C. Bonsignore, H. Paranjape, T. Duerig, J. Mater. Eng. Perform. 2019, 28, 5946.
- [57] L. Yang, H. Yan, J. C. Lam, Appl. Energy 2014, 115, 164.
- [58] F. P. Incropera, D. P. DeWitt, T. L. Bergman, A. S. Lavine, Principles of Heat and Mass Transfer: International Student Version, John Wiley & Sons, Hoboken 2013.
- [59] S. Yoon, M. Kim, J. Seo, S. Kim, H. Lee, J. Lee, B. J. Lee, Energy Build. 2021, 241, 110921.
- [60] M. Kottek, J. Grieser, C. Beck, B. Rudolf, F. Rubel, *Meteorol. Z.* 2006, 15, 259.